Mechanisms of Development 160 (2019) 103578

Contents lists available at ScienceDirect

Mechanisms of Development

journal homepage: www.elsevier.com/locate/mod

Initiation and early growth of the skull vault in zebrafish

Michelle Kanther[a,1,2], Alexandra Scalici[b,2], Azman Rashid[b], Kelly Miao[b], Ella Van Deventer[b,c], Shannon Fisher[b,*]

[a] Perelman School of Medicine, University of Pennsylvania, Dept. of Cell and Developmental Biology, Philadelphia, PA, United States of America
[b] Boston University School of Medicine, Department of Pharmacology & Experimental Therapeutics, Boston, MA, United States of America
[c] Boston University, College of Arts and Sciences, United States of America

ARTICLE INFO

Keywords:
Zebrafish
Skull
Osteoblast
Craniofacial development
Confocal microscopy

ABSTRACT

The zebrafish offers powerful advantages as a model system for examining the growth of the skull vault and the formation of cranial sutures. The zebrafish is well suited for large–scale genetic screens, available in large numbers, and continual advances in genetic engineering facilitate precise modeling of human genetic disorders. Most importantly, zebrafish are continuously accessible for imaging during critical periods of skull formation when both mouse and chick are physically inaccessible. To establish a foundation of information on the dynamics of skull formation, we performed a longitudinal study based on confocal microscopy of individual live transgenic zebrafish. Discrete events occur at stereotyped stages in overall growth, with little variation in timing among individuals. The frontal and parietal bones initiate as small clusters of cells closely associated with cartilage around the perimeter of the skull, prior to metamorphosis and the transition to juvenile fish. Over a period of ~30 days, the frontal and parietal bones grow towards the apex of the skull and meet to begin suture formation. To aid in visualization, we have generated interactive three–dimensional models based on the imaging data, with annotated cartilage and bone elements. We propose a framework to conceptualize development of bones of the skull vault in three phases: initiation in close association with cartilage; rapid planar growth towards the apex of the skull; and finally overlapping to form sutures. Our data provide an important framework for comparing the stages and timing of skull development across model organisms, and also a baseline for the examination of zebrafish mutants affecting skull development. To facilitate these comparative analyses, the raw imaging data and the models are available as an online atlas through the FaceBase consortium (facebase.org).

1. Introduction

Zebrafish is the vertebrate organism best suited for forward genetic screens, many of which have identified mutations affecting aspects of skull or general skeletal development (Haffter et al., 1996; Neuhauss et al., 1996; Piotrowski et al., 1996; Schilling et al., 1996), including some that accurately model human skeletal diseases (Fisher et al., 2003; Huitema et al., 2012; Laue et al., 2008; Laue et al., 2011; Vanoevelen et al., 2011). Genetic engineering tools have facilitated creation of additional zebrafish mutants designed to test gene requirements or model human craniofacial disorders (Kague et al., 2016; Teng et al., 2018). Detailed descriptions of zebrafish skull development have largely focused on the base of the skull and derivatives of the pharyngeal arches, the elements of which are established during the larval period, within the first week of development (DeLaurier et al., 2014; Kimmel et al., 2003; Kimmel et al., 2010). In contrast, the vault of the skull forms over a period of several weeks, with bones not completely covering the brain until late juvenile stages (Cubbage and Mabee, 1996; Grova et al., 2012; Laue et al., 2011; Quarto and Longaker, 2005). While these stages in zebrafish skull formation have not been described in detail, overall the morphogenetic events are similar to those in other model organisms, including mouse (Van Otterloo et al., 2016).

Previous descriptions of skull vault development in zebrafish have been largely based on Alizarin red staining, a relatively late marker of bone formation that detects mineralization. This approach fails to take advantage of two major advantages of zebrafish—its accessibility for dynamic imaging of live animals throughout development; and the availability of a large number of fluorescently labeled transgenic lines.

* Corresponding author.
E-mail address: shanfish@bu.edu (S. Fisher).
[1] Current address: University of the Sciences, Dept. of Biological Sciences, Philadelphia, PA, United States of America.
[2] These authors contributed equally.

https://doi.org/10.1016/j.mod.2019.103578
Received 21 August 2019; Received in revised form 24 September 2019; Accepted 3 October 2019
Available online 20 October 2019
0925-4773/

Using transgenic lines that fluorescently label cartilage and bone, we have developed an approach to observe the dynamics of skull formation with low–magnification confocal microscopy. Using these new tools, we can image individual fish sequentially over the entire period of skull vault formation, acquiring an unprecedented level of detailed information about initiation and growth of the frontal and parietal bones. To maximize the utility of these data, the original confocal files are available online as part of the FaceBase consortium (Brinkley et al., 2016). In addition, we have constructed three-dimensional annotated models for a subset of the data, in an accessible interactive PDF format. Together, these data and accompanying models provide a foundation for quantitative analysis of mutant phenotypes, and suggest a framework for considering the cellular events underlying skull morphogenesis.

2. Materials and methods

2.1. Animal husbandry

Fish were maintained according to standard protocols (Westerfield, 2007). Studies were conducted in strict accordance with the Guide for the Care and Use of Laboratory Animals of the National Institutes of Health. All experiments were performed using protocols approved by the Institutional Animal Care and Use Committees at Boston University and the University of Pennsylvania. The transgenic line *Tg(-1.4col1a1:egfp)*, hereafter referred to as *col1a1:egfp*, has been previously described (Kague et al., 2012). Transgenic fish expressing mCherry under control of medaka *sp7* regulatory sequences, referred to as *sp7:mcherry* (Kague et al., 2016), were generated using the *osterix-mcherry*-BSIISK-ISce-I plasmid (Renn and Winkler, 2009), kindly provided by Christoph Winkler. Plasmid and *Sce*I enzyme were injected into zebrafish embryos at the one cell stage to generate founders, as previously described (Soroldoni et al., 2009; Thermes et al., 2002).

2.2. Staging and standard length measurements

Zebrafish were anesthetized with Tricaine (MS-222, Sigma-Aldrich), mounted in 3% methylcellulose and imaged using an Olympus MVX10 stereomicroscope with a DP72 camera. Fish were staged by developmental landmarks and length measurements determined as a proxy for developmental stage, as previously described (Parichy et al., 2009).

2.3. In vivo imaging

Zebrafish were anesthetized with Tricaine (MS-222, Sigma-Aldrich), and mounted in 2% low melt SeaPlaque agarose (Lonza) on glass bottom dishes (MatTex Corporation). Solidified agarose blocks containing fish were covered in E3 media. Agarose covering gills and mouth was carefully carved away using a dissecting probe to allow for respiration. Confocal image acquisition took ~10 min, after which fish were released from the agarose and returned to the facility. Images were captured daily during initiation and early growth of the frontal bones; as the fish became larger and the rate of growth slowed, images were acquired every 2–5 days. Images were captured using a Leica TCS-LSI III macro-confocal microscope with 2× and 5× Plan APO objectives, generating .lif files. These were converted to .tiff files in Fiji/ImageJ (version 2.0.0) for further processing.

2.4. Bone area quantification

For each time point and each fish, maximum intensity projections of the *sp7:mCherry* expression were generated in Fiji. These were processed (despeckled) to reduce noise, and threshold adjusted to isolate bone areas of interest from background. Frontal bone areas were further refined manually through edge tracing, and selected areas measured.

2.5. Three–dimensional modeling of skull elements and creation of PDFs

For each confocal stack, the two channels (GFP and mCherry) were saved separately, along with their respective metadata. The files were further processed in Amira (FEI version 6.4.0). Briefly, a deconvolution module was attached to the data to remove scattered light. Next, a median filter was applied to smooth out signal among neighboring voxels. A multi-thresholding module was used to draw the boundary between exterior and interior expression signal. In the segmentation editor tab in Amira, the paintbrush and other tools were used to manually segment all bone and cartilage regions of interest. Each highlighted region was then saved to the material list. After segmentation, the general surface module was used to generate the corresponding merged bone and cartilage 3D surface from the mCherry and GFP label data. The surface file (.surf format) can be visualized in Amira and exported to other formats. To generate 3D PDFs, each surface was imported to a blank PDF document using the rich media tool in Adobe Acrobat Pro DC. Interactive buttons, using Javascript, were added to show, hide and make transparent the sub-objects in the surface, corresponding to individual bones and cartilage elements. Unix and Fiji macro scripts were written for batch processing of larger image datasets.

3. Results

3.1. Imaging of transgenic fish reveals earliest sites of skull bone formation

Previous studies of vertebrate skull development have been largely limited to observations of single time points of individual animals, fixed and stained. We have developed methods to visualize the dynamics of skull development over time in individual live zebrafish. We relied on expression of two previously reported transgenes, *col1a1:egfp* and *sp7:mcherry* (Fig. 1). The *col1a1:egfp* transgene is expressed in the cartilage elements by 4dpf, well before initiation of the bones of the skull vault (Kague et al., 2012). This expression provides an anatomical context in which to visualize bone development. The *sp7:mcherry* transgene is expressed in osteoblasts of developing bones during osteogenesis (Kague et al., 2016). Use of a transgenic reporter enables earlier visualization of bone prior to mineralization, and allows direct visualization of the cells rather than the surrounding matrix.

Although the developmental timing of the branchial arch derived skeleton has been well described in zebrafish, the relative developmental timing of the skull vault has not been well characterized. To more precisely define the developmental stages associated with skull vault development, we performed live imaging of individual wildtype *Tg(col1a1:egfp; sp7:mCherry)* zebrafish beginning prior to the appearance of the frontal bone and continuing through suture formation. Through larval stages, zebrafish are amenable to standard confocal imaging in laser scanning or spinning disk systems. However, by the stage at which the frontal bone begins to form, the fish have exceeded practical size limits for standard systems based on compound microscope optics, which have small physical working distances and limited imaging depth. To accommodate these larger specimens, the macro-confocal system we used to acquire images has a working distance of ≥ 20 mm, and maximum imaging depth of > 200 µm, and a field of view large enough to encompass the entire skull in a single image.

Just prior to formation of the frontal bones, in fish at the stage of metamorphic melanophore appearance (MMA), the perimeter of the skull is encircled (from anterior to posterior) by the taenia marginalis anterior and posterior (TMA, TMP), and the tectum synotium (TS) cartilage elements. The epiphyseal bar cartilage (EPB) bridges the left and right sides, crossing above the brain (Fig. 1b). Skull vault development is first visible as early clusters of *sp7:mcherry* positive osteoblasts of the frontal bone in close association with the TMP in fish at the stage of anterior swim bladder appearance (aSB) (Figs. 2a and 3). Following this initial appearance of cells, early frontal bone growth

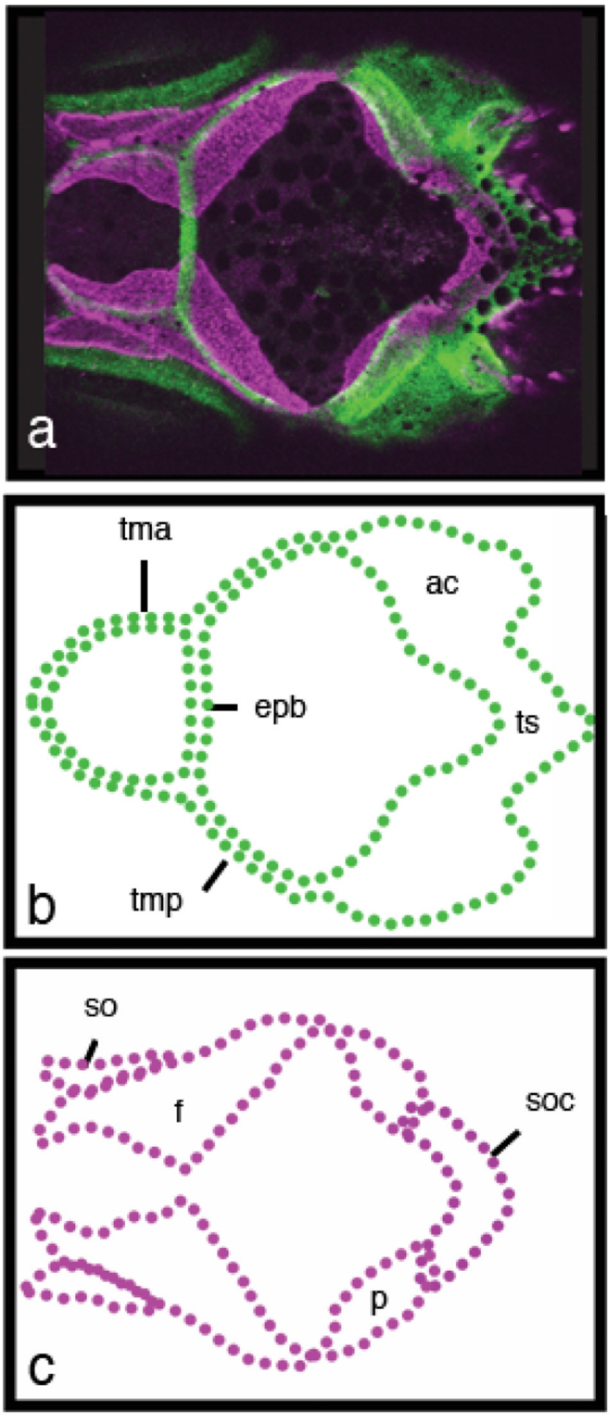

Fig. 1. *Tg(col1a1:egfp; sp7:mcherry)* zebrafish as live indicators of skeletal development. (a) Maximum projection of z-stack of confocal images of live *Tg (col1a1:egfp; sp7:mCherry)* zebrafish. Schematic depictions of (b) cartilage structures marked by *col1a1:egfp* transgene and (c) bone marked by *sp7:mcherry* transgene. Abbreviations: taenia marginalis anterior (tma), epiphyseal bar (epb), taenia marginalis posterior (tmp), auditory capsule (ac), tectum synoticum (ts), supraorbital bone (so), frontal bone (f), parietal bone (p), and supraoccipital bone (soc).

continues in close association with cartilage, extending along the length of the TMP, crossing the EPB, and continuing along TMA (Fig. 2a). The close association of osteoblasts with cartilage is especially apparent in 3-dimensional renderings of the confocal stacks (Supplemental movies). In individual fish, frontal bone initiation was observed first on either the left or right side (Fig. 2B). The data from all individuals in which we could capture initiation suggested a bias towards initiation on the left side (13/20). However, the sample size provided insufficient statistical power to rule out random initiation.

3.2. Sequential live imaging shows phases of skull bone growth

To more precisely characterize the remaining stages of skull vault development we continued imaging individual *Tg(col1a1:egfp; sp7:mcherry)* zebrafish throughout skull development into the early formation of the sutures (Fig. 3). In fish at the stage of dorsal fin ray appearance (DR), frontal bones begin to extend towards the apex of the skull in a planar phase of growth, with the leading edge of the growing bones extending along the top of the EPB (Fig. 3). Similar to our observations of frontal bone initiation, we find that cells of the parietal bones are first observed in close proximity to a cartilage element, the TS, beginning in fish at the stage of pelvic fin bud appearance (PB) (Fig. 3). The phase of rapid planar growth terminates with the formation of the coronal, metopic and sagittal sutures. We observed the formation of these sutures beginning in fish at the stage of squamation through anterior (SA), with clear overlap by juvenile stages (Fig. 3).

The repeated anesthesia, handling, and imaging we use to follow skull growth in individual fish have the potential to adversely affect their developmental trajectory. While we did sometimes observe overall growth retardation in fish that were imaged many times relative to fish of the same age in our facility, we also found that the overall relationship between developmental stages and the appearance and growth of the skull bones remained consistent. We also observe a fairly high mortality rate during long–term imaging experiments. Although it is possible that the fish are sensitized by repeated anesthesia, it is difficult to separate out that effect from the generally increased sensitivity that older fish show towards Tricaine. It is possible that alternative methods of anesthesia could reduce mortality in the older fish and facilitate longer imaging experiments.

3.3. Quantification of frontal bone areas as a function of overall growth

To quantify bone growth over developmental time we determined frontal bone area (mCherry positive) from compressed z-stacks, measured in 25 wild–type animals from four separate experiments (Fig. 4). The areas of left and right frontal bones for each fish were averaged and plotted as a single point. We also measured each fish and used standard length (SL) as a proxy for developmental stage, allowing us to plot bone area as a function of SL and perform statistical analyses. The smallest fish in which we detected frontal bone osteoblasts was 5.45 mm SL, and the largest in which we did not see any was 5.83 mm, defining the normal range of first detection of osteoblasts; the smallest area measured was 150.22 μm^2 (Fig. 4a). During the first several days after the first appearance of frontal bone osteoblasts, there is relatively little change in the bone area; up to 6.1 mm SL, bone is added at a rate of 0.051 mm^2/mm SL (Fig. 4b). During the subsequent period of rapid planar growth, bone area is tightly correlated with SL (R^2 = 0.91), and is added at a rate of 0.13 mm^2/mm SL. This corresponds to a rate of new bone addition of ~0.025 mm^2/day, although the correlation is better with standard length, consistent with normal variations in growth observed under different rearing conditions. In the final growth phase, when the frontal bones come in contact and sutures begin to form (> 10.0 mm SL), the rate of new bone addition slows to 0.093 mm^2/mm SL.

3.4. Three–dimensional visualization of skull structure in development

To aid in visualization of the complex structures and their interrelationships during skull development, we created annotated models at three selected stages. At each stage, the confocal stacks for chondrocytes (expressing GFP) and osteoblasts (expressing mCherry) were processed separately, as described in the Methods. Using a combination

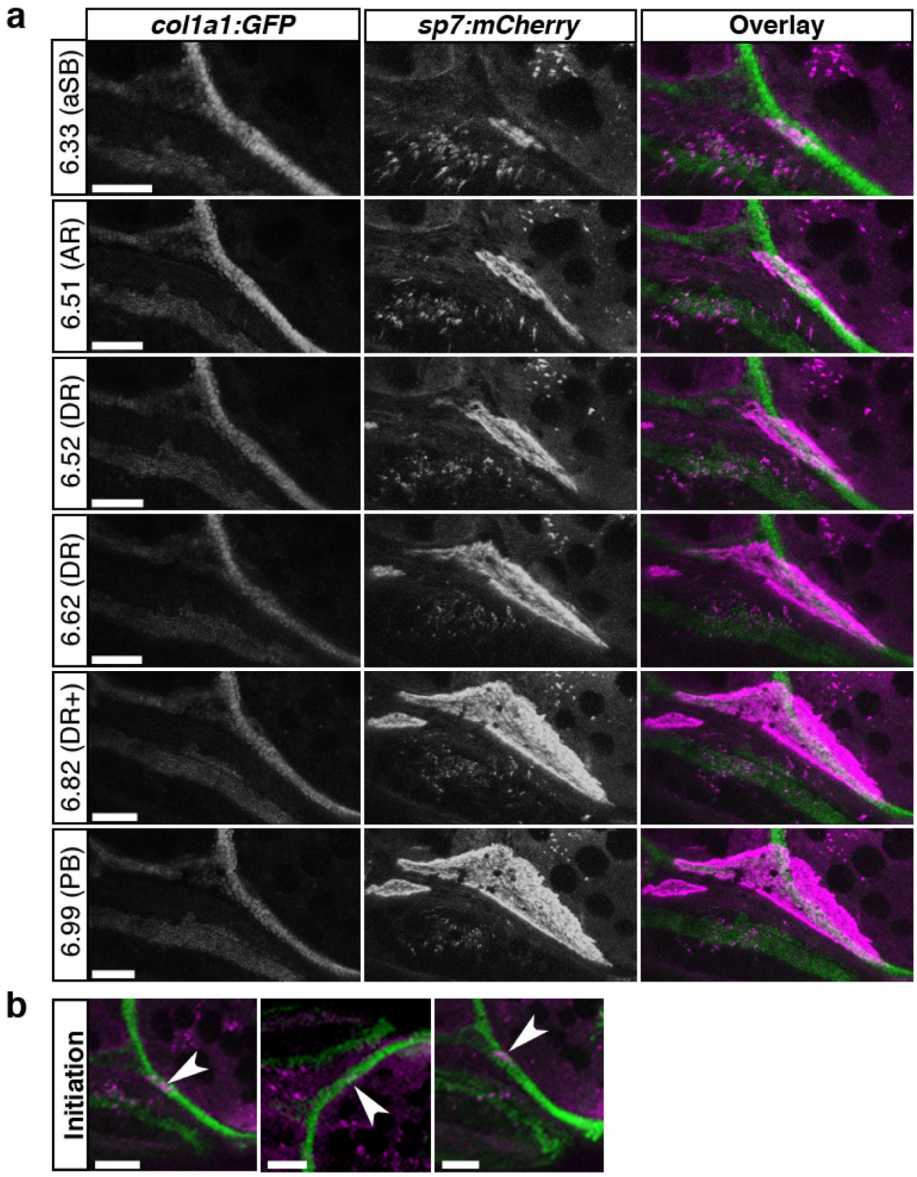

Fig. 2. Confocal imaging of frontal bone initiation. (a) High magnification fluorescent imaging of live *Tg (col1a1:egfp; sp7:mcherry)* zebrafish illustrates close association of bone initiation with cartilage. Each set of panels represents maximum projections of z-stacks, separate GFP and mCherry channels and the overlay. Beside each panel, the standard length (SL) in mm is listed, with the developmental staging in parentheses, according to Parichy et al. (2009). At 6.33 mm SL the first osteoblasts are seen in close proximity with TMP. Bone growth initiates along TMP before crossing EPB and continuing along TMA. Frontal bone begins planar growth away from cartilage at 6.82 mm SL. (b) Examples from three individual fish illustrate initiation of frontal bone on either left or right side (arrowheads). Abbreviations: anterior swim bladder appearance (aSB); anal fin ray appearance (AR); dorsal fin ray appearance (DR); pelvic fin bud appearance (PB). Scale bars = 100 µm.

of automated and manual segmentation, three-dimensional objects were generated for each individual bone and cartilage element. These were color-coded and annotated, and the files merged for each stage (Fig. 5). To create the final PDF models, functional buttons were added allowing each element to be made translucent or entirely transparent; the entire model can be rotated freely and zoomed to lower or higher magnification. The PDFs are available for download as supplemental files.

4. Discussion

We present here the first description of the dynamic events of skull formation in a model organism. During the critical period of skull vault formation, mouse and chick are inaccessible for imaging. We have used low–magnification confocal microscopy of transgenic zebrafish to describe the dynamics of skull vault formation, affording a three–dimensional view of the complex skull structures and their changing interrelationships during development.

The rate of zebrafish development and growth is sensitive to environmental factors, including temperature, diet, and culture density. For consistency of staging, developmental landmarks should be used rather than times post fertilization; therefore, we present our data based on previously published standards for post–larval staging (Parichy et al., 2009). Through sequential imaging of multiple fish, we have also quantified growth of the frontal bones, using standard length as a proxy for developmental stage. Our data provide a framework whereby to evaluate the same processes in zebrafish mutants in future studies. They also allow more direct comparisons with skull growth in other organisms, including chick, mouse, and even human.

We observe the first evidence of osteoblasts of the frontal bone at the aSB stage, corresponding to 12–16 days post fertilization in our rearing conditions. This is considerably earlier than previous descriptions, which relied on Alizarin red to detect mineralized bone (Cubbage and Mabee, 1996; Topczewska et al., 2016). In the initiation phase, we observe small clusters of osteoblasts in close association with cartilage elements around the periphery of the skull (TMP for the frontal bones, TS for the parietal). In the case of the frontal bones, over the next several days the group of cells expands, but still remains closely associated with cartilage. The bones of the skull vault are generally considered to be intramembranous bones, forming in the absence of a cartilage template. Our observations, however, suggest that initiation of these bones relies on cartilage, perhaps blurring the distinction between membranous and perichondral bones during development.

After the initiation phase, the frontal bones (and with a lag of

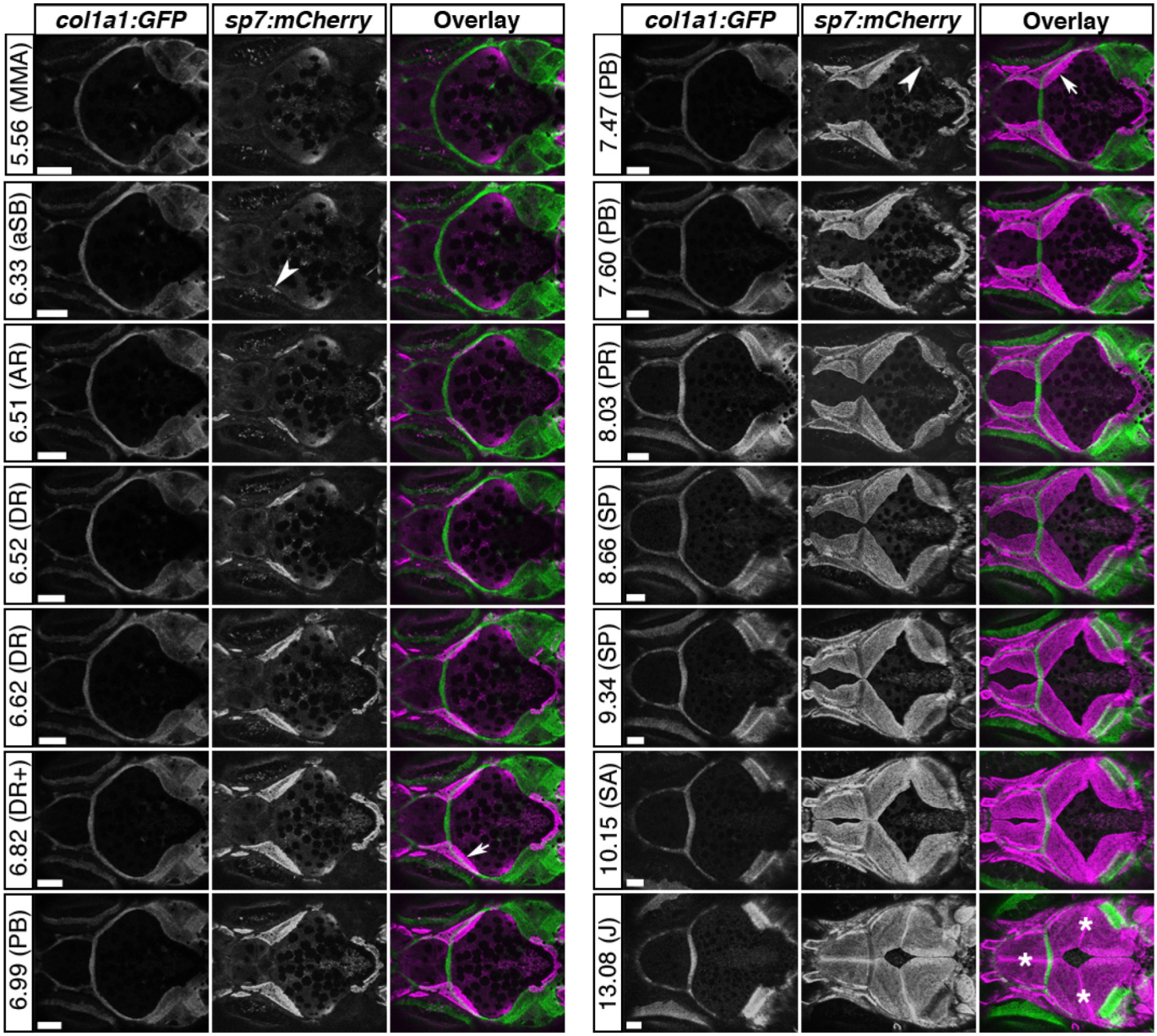

Fig. 3. Sequential live imaging of skull vault development. Confocal images are shown for a single *Tg(col1a1:egfp; sp7:mcherry)* zebrafish during the entire period of skull vault formation, with corresponding SL measurements in mm, and developmental staging in parentheses as in Fig. 2. Each set of panels represents maximum projections of z-stacks, separate GFP and mCherry channels and the overlay. Notable events are frontal bone initiation (arrowhead at 6.33 mm), planar bone growth towards apex of skull (arrows), parietal bone initiation (arrowhead at 7.47 mm), and suture formation (asterisks). Abbreviations as in Fig. 2, plus: metamorphic melanophore appearance (MMA); squamation onset posterior (SP); squamation through anterior (SA); juvenile (J). Scale bars = 100 μm.

several days, the parietal bones) enter a phase of rapid planar growth towards the apex of the skull. Interestingly, the leading edge of frontal bone growth in this phase is along the top of the EPB cartilage, again suggesting an important role of the cartilage in supporting or guiding growth. Finally, the bones meet at the apex and overlap at the edges to form sutures (metopic or interfrontal, coronal, and sagittal). At this point, the skull vault has assumed essentially its adult morphology, although it will grow considerably to achieve adult size. By analogy with the widely accepted model of skull growth in mammals, new bone area is added primarily at the osteogenic fronts at the sutures (Teng et al., 2018; Topczewska et al., 2016), consistent also with a concentration of mitotically active cells at the osteogenic fronts (Kague et al., 2016).

Previous studies have shown that the frontal bones are of mixed embryological origin (Kague et al., 2012; Mongera et al., 2013). The anterior portion shows extensive neural crest contribution, while the posterior portion has negligible neural crest and is presumably derived from mesoderm. Interestingly, the division between the two portions lies on top of the EPB. The frontal bones of the chicken are of similar mixed origin, and it has been suggested that they arise from two separate centers of ossification that subsequently fuse into one bone (Evans and Noden, 2006). By analogy, we might predict two separate groups of precursor cells for the frontal bone in zebrafish, but in fact we see no evidence of that. At every stage examined from the first appearance of osteoblasts, we observed only one continuous group of cells contributing to the frontal bone on each side. Our studies provide the foundation for future experiments where genetic lineage tracing, in conjunction with similar confocal imaging, will reveal the origin of the earliest cells of the frontal bone. This information will help construct hypotheses explaining how cells of two different origins are recruited

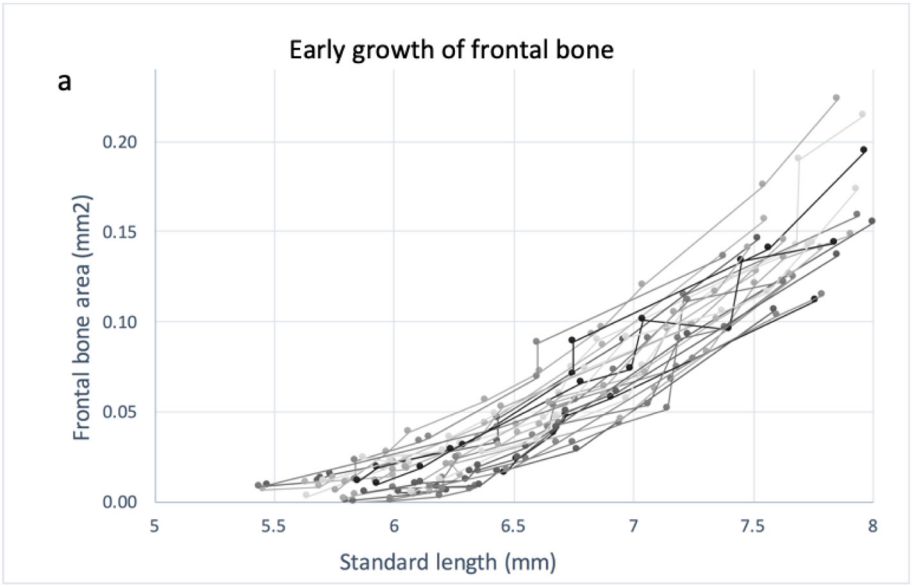

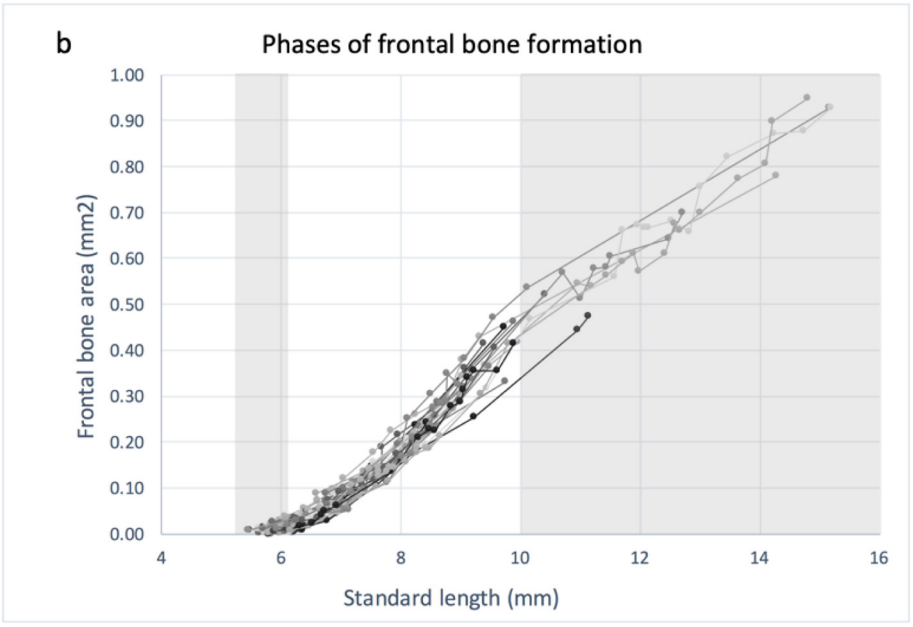

Fig. 4. Frontal bone initiation and growth is tightly correlated with developmental milestones. Frontal bone area was measured for 25 individual fish, and plotted as a function of standard length in mm. (a) Frontal bone area during initiation and early growth (5.5–8.0 mm SL) is shown for all individuals, to illustrate the variation in timing of first appearance of osteoblasts and in the growth rate. (b) Frontal bone growth is shown for the entire measurement period, with each line tracing the growth data from an individual fish; the three phases of growth we have defined are indicated by shading (initiation: gray; planar growth: white; and suture formation: gray).

into the bone and why the boundary is located precisely over the EPB.

Complex three-dimensional interactions among several tissues are coordinated during normal skull formation. These are challenging to visualize, and there is little quantitative data available for normal patterns of growth in any species. It is also difficult in the absence of detailed developmental descriptions to draw parallels among organisms with respect to identity of bone and cartilage elements. This is especially critical as the use of model organisms to reproduce human craniofacial defects becomes more common, to determine whether parallel genetic changes in a model organism produce similar defects. To facilitate the wide use of our data, many of the confocal images have been deposited on the FaceBase web site (Brinkley et al., 2016), where the data is freely available for download. In addition, we have generated annotated models of several select stages, to serve as an atlas and aid in visualization. These models, available for download as supplements to this paper, will also be available for online viewing on FaceBase through an integrated object viewer.

In addition to hosting zebrafish data from our lab and others, the FaceBase site serves as a repository for morphological data on mouse skull development; on human craniofacial dysmorphology; and genomics data sets on a variety of species relevant to craniofacial development. As such, it facilitates the detailed comparative studies necessary to develop zebrafish models of craniofacial disorders. Our data in particular will serve as an important benchmark of normal skull formation, against which future mutants can be measured.

Acknowledgments

The authors would like to thank the staff of the aquatics facilities at the University of Pennsylvania and Boston University for their care of our fish stocks. The work was supported by grants U01 DE024434 and R01 DE022955 to S. F. from NIH NIDCR.

Appendix A. Supplementary data

Supplementary data to this article can be found online at https://doi.org/10.1016/j.mod.2019.103578.

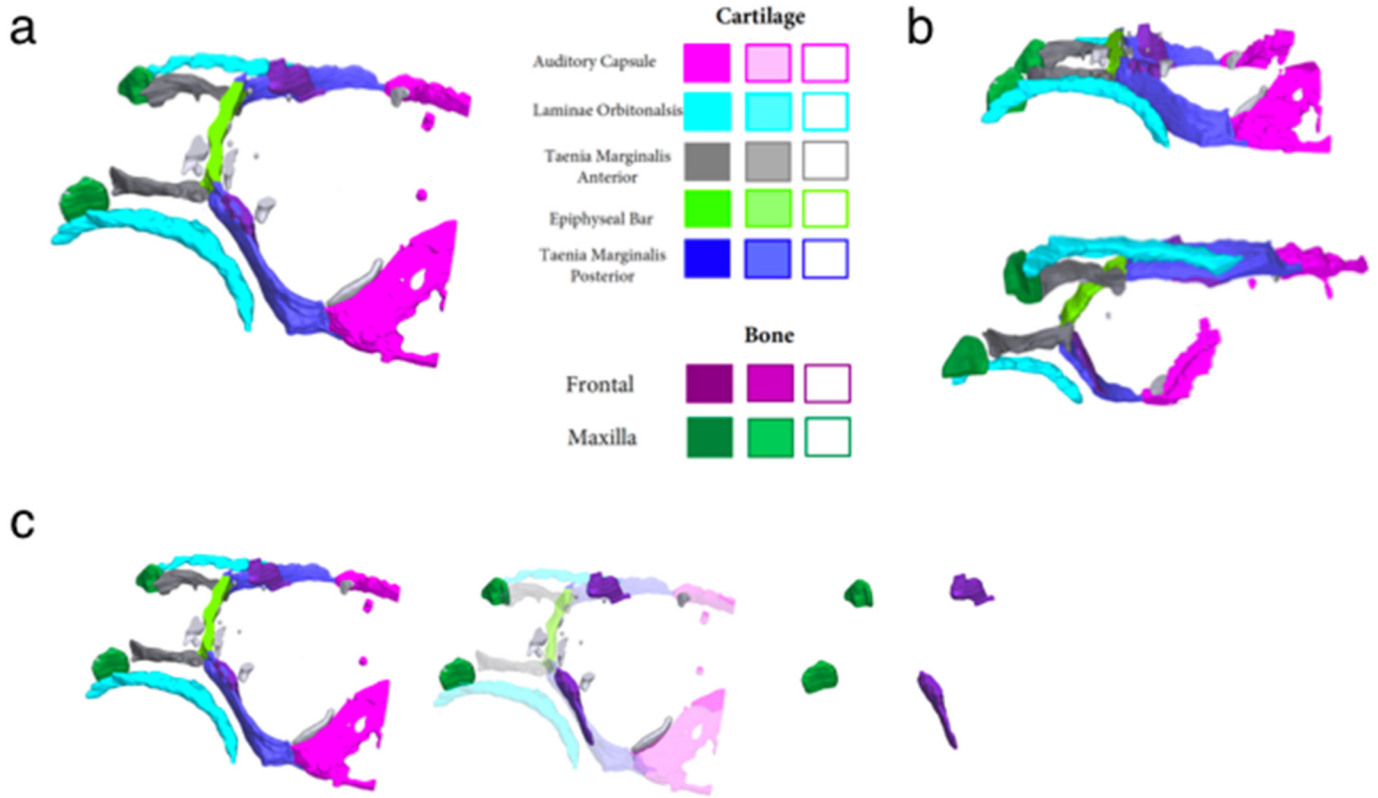

Fig. 5. Three dimensional models of skull morphogenesis. At selected stages in normal skull formation, the confocal imaging data was used to generate interactive PDFs. (a) In each file, individual bones and cartilage elements are color-coded and labeled. The images can be rotated freely (b), and each element can be made translucent or transparent independently (c).

References

Brinkley, J.F., Fisher, S., Harris, M.P., Holmes, G., Hooper, J.E., Jabs, E.W., Jones, K.L., Kesselman, C., Klein, O.D., Maas, R.L., Marazita, M.L., Selleri, L., Spritz, R.A., van Bakel, H., Visel, A., Williams, T.J., Wysocka, J., FaceBase, C., Chai, Y., 2016. The FaceBase Consortium: a comprehensive resource for craniofacial researchers. Development 143, 2677–2688.

Cubbage, C.C., Mabee, P.M., 1996. Development of the cranium and paired fins in the zebrafish Danio rerio (Ostariophysi, Cyprinidae). J. Morphol. 229, 121–160.

DeLaurier, A., Huycke, T.R., Nichols, J.T., Swartz, M.E., Larsen, A., Walker, C., Dowd, J., Pan, L., Moens, C.B., Kimmel, C.B., 2014. Role of mef2ca in developmental buffering of the zebrafish larval hyoid dermal skeleton. Dev. Biol. 385, 189–199.

Evans, D.J., Noden, D.M., 2006. Spatial relations between avian craniofacial neural crest and paraxial mesoderm cells. Dev. Dyn. 235, 1310–1325.

Fisher, S., Jagadeeswaran, P., Halpern, M.E., 2003. Radiographic analysis of zebrafish skeletal defects. Dev. Biol. 264, 64–76.

Grova, M., Lo, D.D., Montoro, D., Hyun, J.S., Chung, M.T., Wan, D.C., Longaker, M.T., 2012. Models of cranial suture biology. J. Craniofac. Surg. 23, 1954–1958.

Haffter, P., Odenthal, J., Mullins, M.C., Lin, S., Farrell, M.J., Vogelsang, E., Haas, F., Brand, M., van Eeden, F.J., Furutani-Seiki, M., Granato, M., Hammerschmidt, M., Heisenberg, C.P., Jiang, Y.J., Kane, D.A., Kelsh, R.N., Hopkins, N., Nüsslein-Volhard, C., 1996. Mutations affecting pigmentation and shape of the adult zebrafish. Dev. Genes Evol. 206, 260–276.

Huitema, L.F., Apschner, A., Logister, I., Spoorendonk, K.M., Bussmann, J., Hammond, C.L., Schulte-Merker, S., 2012. Entpd5 is essential for skeletal mineralization and regulates phosphate homeostasis in zebrafish. Proc. Natl. Acad. Sci. U. S. A. 109, 21372–21377.

Kague, E., Gallagher, M., Burke, S., Parsons, M., Franz-Odendaal, T., Fisher, S., 2012. Skeletogenic fate of zebrafish cranial and trunk neural crest. PLoS One 7, e47394.

Kague, E., Roy, P., Asselin, G., Hu, G., Simonet, J., Stanley, A., Albertson, C., Fisher, S., 2016. Osterix/Sp7 limits cranial bone initiation sites and is required for formation of sutures. Dev. Biol. 413, 160–172.

Kimmel, C.B., Ullmann, B., Walker, M., Miller, C.T., Crump, J.G., 2003. Endothelin 1-mediated regulation of pharyngeal bone development in zebrafish. Development 130, 1339–1351.

Kimmel, C.B., DeLaurier, A., Ullmann, B., Dowd, J., McFadden, M., 2010. Modes of developmental outgrowth and shaping of a craniofacial bone in zebrafish. PLoS One 5, e9475.

Laue, K., Jänicke, M., Plaster, N., Sonntag, C., Hammerschmidt, M., 2008. Restriction of retinoic acid activity by Cyp26b1 is required for proper timing and patterning of osteogenesis during zebrafish development. Development 135, 3775–3787.

Laue, K., Pogoda, H.M., Daniel, P.B., van Haeringen, A., Alanay, Y., von Ameln, S., Rachwalski, M., Morgan, T., Gray, M.J., Breuning, M.H., Sawyer, G.M., Sutherland-Smith, A.J., Nikkels, P.G., Kubisch, C., Bloch, W., Wollnik, B., Hammerschmidt, M., Robertson, S.P., 2011. Craniosynostosis and multiple skeletal anomalies in humans and zebrafish result from a defect in the localized degradation of retinoic acid. Am. J. Hum. Genet. 89, 595–606.

Mongera, A., Singh, A.P., Levesque, M.P., Chen, Y.Y., Konstantinidis, P., Nüsslein-Volhard, C., 2013. Genetic lineage labeling in zebrafish uncovers novel neural crest contributions to the head, including gill pillar cells. Development 140, 916–925.

Neuhauss, S.C., Solnica-Krezel, L., Schier, A.F., Zwartkruis, F., Stemple, D.L., Malicki, J., Abdelilah, S., Stainier, D.Y., Driever, W., 1996. Mutations affecting craniofacial development in zebrafish. Development 123, 357–367.

Parichy, D.M., Elizondo, M.R., Mills, M.G., Gordon, T.N., Engeszer, R.E., 2009. Normal table of postembryonic zebrafish development: staging by externally visible anatomy of the living fish. Dev. Dyn. 238, 2975–3015.

Piotrowski, T., Schilling, T.F., Brand, M., Jiang, Y.J., Heisenberg, C.P., Beuchle, D., Grandel, H., van Eeden, F.J., Furutani-Seiki, M., Granato, M., Haffter, P., Hammerschmidt, M., Kane, D.A., Kelsh, R.N., Mullins, M.C., Odenthal, J., Warga, R.M., Nüsslein-Volhard, C., 1996. Jaw and branchial arch mutants in zebrafish II: anterior arches and cartilage differentiation. Development 123, 345–356.

Quarto, N., Longaker, M.T., 2005. The zebrafish (Danio rerio): a model system for cranial suture patterning. Cells Tissues Organs 181, 109–118.

Renn, J., Winkler, C., 2009. Osterix-mCherry transgenic medaka for in vivo imaging of bone formation. Dev. Dyn. 238, 241–248.

Schilling, T.F., Piotrowski, T., Grandel, H., Brand, M., Heisenberg, C.P., Jiang, Y.J., Beuchle, D., Hammerschmidt, M., Kane, D.A., Mullins, M.C., van Eeden, F.J., Kelsh, R.N., Furutani-Seiki, M., Granato, M., Haffter, P., Odenthal, J., Warga, R.M., Trowe, T., Nüsslein-Volhard, C., 1996. Jaw and branchial arch mutants in zebrafish I: branchial arches. Development 123, 329–344.

Soroldoni, D., Hogan, B.M., Oates, A.C., 2009. Simple and efficient transgenesis with meganuclease constructs in zebrafish. Methods Mol. Biol. 546, 117–130.

Teng, C.S., Ting, M.C., Farmer, D.T., Brockop, M., Maxson, R.E., Crump, J.G., 2018. Altered bone growth dynamics prefigure craniosynostosis in a zebrafish model of Saethre-Chotzen syndrome. Elife 7.

Thermes, V., Grabher, C., Ristoratore, F., Bourrat, F., Choulika, A., Wittbrodt, J., Joly, J.S., 2002. I-SceI meganuclease mediates highly efficient transgenesis in fish. Mech. Dev. 118, 91–98.

Topczewska, J.M., Shoela, R.A., Tomaszewski, J.P., Mirmira, R.B., Gosain, A.K., 2016. The morphogenesis of cranial sutures in zebrafish. PLoS One 11, e0165775.

Van Otterloo, E., Williams, T., Artinger, K.B., 2016. The old and new face of craniofacial research: how animal models inform human craniofacial genetic and clinical data. Dev. Biol. 415, 171–187.

Vanoevelen, J., Janssens, A., Huitema, L.F., Hammond, C.L., Metz, J.R., Flik, G., Voets, T., Schulte-Merker, S., 2011. Trpv5/6 is vital for epithelial calcium uptake and bone formation. FASEB J. 25, 3197–3207.

Westerfield, M., 2007. The Zebrafish Book.